Steam reforming of ethanol–phenol mixture on Ni/Al$_2$O$_3$: Effect of magnesium and boron on catalytic activity in the presence and absence of sulphur

Gabriella Garbarino[a], Elisabetta Finocchio[a,*], Alberto Lagazzo[a], Ioannis Valsamakis[b], Paola Riani[c], Vicente Sanchez Escribano[d], Guido Busca[a]

[a] Dipartimento di Ingegneria Civile, Chimica e Ambientale, Laboratorio di Chimica delle Superfici e Catalisi Industriale, Università di Genova, P.le J.F. Kennedy 1, I-16129, Genova, Italy
[b] Department of Chemical and Biological Engineering, Tufts University, Medford, MA, USA
[c] Dipartimento di Chimica e Chimica Industriale, Università di Genova, Via Dodecaneso 31, I-16146 Genova, Italy
[d] Departamento de Quimica Inorganica, Universidad de Salamanca, Salamanca, Spain

ARTICLE INFO

ABSTRACT

The steam reforming of ethanol/phenol mixture (168 g$_{TOT}$/N m^3, ethanol: phenol 2:1 mol), assumed as a model for tar mixtures, has been studied over Ni/Al$_2$O$_3$, Ni-Mg/Al$_2$O$_3$ and Ni-B/Al$_2$O$_3$ catalysts. The effects of reaction temperature and of the presence of sulphur have been investigated. Catalysts have been characterized by XRD, IR of adsorbed CO, TPR, UV–vis spectroscopies. IR studies of adsorbed water and phenol have also been performed.

The addition of Magnesium shows an activating effect on Ni/Al$_2$O$_3$ but also increases sensitivity to sulphur poisoning. This has been associated to the formation of large Ni metal particles over the Mg$_x$Al$_2$O$_{3+x}$ support surface formed by the penetration of Mg ions in the subsurface of alumina, and to the low activity of the surface of such a modified support in the conversion of the organic reactants. A possible role of Mg in a different, possibly more efficient, activation of water is envisaged. The addition of boron in small amounts reduces activity, mainly if boron is added to the support before impregnation of Ni. A slight positive effect in reducing the deactivation due to sulphur is observed when boron is added after nickel.

© 2013 Elsevier B.V. All rights reserved.

1. Introduction

Supported nickel catalysts are largely used in industry in several different fields. In particular, they are used for hydrogenations carried out at relatively low temperatures (473–773 K), such as methanation [1,2] and full saturation of aromatics [3] and dienes [4,5]. In this case medium/high surface area transitional aluminas (γ-, η- or θ-Al$_2$O$_3$) are commonly used as catalyst supports. Supported nickel is also used for steam reforming of natural gas, including prereforming, autothermal reforming and secondary reforming [6,7]. According to the thermodynamics, these reactions are carried out at considerably higher temperatures (873–1173 K), thus stable refractory carriers, such as corundum alumina (α-Al$_2$O$_3$), Mg aluminate spinels (MgAl$_2$O$_4$) or Ca-based aluminates (CaAl$_{12}$O$_{19}$, CaAl$_{22}$O$_{34}$ β-aluminas) are used. In some cases, silica is also employed as a morphology stabilizer of the catalyst support. In all cases, Ni based catalysts are applied industrially although they

suffer from deactivation due to coking, sulphur poisoning, sintering and re-oxidation of the metal phase [6].

The steam reforming of ethanol [8] as well as the steam reforming of biomass tar [9,10] are new technologies with potential industrial interest, that can be performed at intermediate temperatures (673–1073 K) using Ni-based catalysts. In these conditions, the stabilization of the carrier morphology might be less relevant, but increasing the activity and, in particular, reducing the catalyst deactivation, are certainly key factors. Depending on the process configuration and the raw materials Ni catalysts for tar abatement may compete with the noble metal-based catalysts, such as rhodium-based catalysts [11] which may be more active at low temperature and more resistant to sulphur, but they are certainly more expensive.

It is well known that alkali and alkali earth cations moderate the surface acidity of alumina and can also induce surface basicity [12,13]. Thus besides acting as structural stabilizers of the support, they might also limit the catalyst coking. Several studies suggest that these components, namely magnesium, may also increase the catalytic activity of Ni/Al$_2$O$_3$, e.g. for ethanol steam reforming [14] and for methane reforming [15], with Ni/MgAl$_2$O$_4$ acting as

excellent tar steam reforming catalysts [16]. Literature data also report on a positive effect of small amounts of boron (0.5 and 1 wt%), which is found to enhance the stability of Ni/Al_2O_3 catalyst in methane steam reforming, and limit coking, without compromising the activity [17]. In addition, adding boron in such a low concentration range is also known to reduce sulphur deactivation of Ni/SiO_2 hydrogenation catalysts [18].

We investigated recently the conversion of a mixture of ethanol and phenol, as a model of biomass tar mixture, with steam over Ni/Al_2O_3 catalysts [19,20]. We confirmed the high catalytic activity of these catalysts and their poisoning by sulphur, but also the possibility of their partial regeneration. In this paper we report on our attempts to further improve the catalytic activity and the sulphur resistance of these Ni/Al_2O_3 catalysts by adding Mg and B as stabilizers.

2. Experimental

2.1. Catalysts preparation

Catalysts (Table 1) have been prepared by wet impregnation procedures using water solutions of $Ni(NO_3)_2 \cdot 6H_2O$, $Mg(NO_3)_2 \cdot 6H_2O$, and $B(OH)_3$ and Siralox 5/170 (Sasol, 95% Al_2O_3, 5% SiO_2, with traces of iron and sodium as impurities) as the support. The support itself will be denoted as NiØ. The presence of silica is useful to increase the stability of transitional alumina towards phase transition. Loadings of both Mg and B have been chosen following literature results [14,17,18]. All impregnation steps were followed by drying and calcination at 973 K for 5 h. NiMg catalyst was prepared by sequential impregnation of Mg, first, and Ni later. The bare support MgO 20% (w/w) on Siralox is denoted MgNiØ.

In preparing NiB catalyst, first boron was impregnated, Ni later. The reverse for BNi.

2.2. Catalysts characterization

A modified Sartorius symmetrical microbalance, described elsewhere [21], was used for the determination of the specific surface area and of the pore size distribution. About 50 mg of powder was placed in a Pt crucible and introduced in the microbalance. The sample was dried at 383 K in vacuum (10^{-4} Pa) and, after the weight was stabilized at the microbalance sensitivity (0.01 mg), was cooled at 78 K without removing it from the crucible and without air contamination. N_2 gas was introduced step by step in the apparatus until a maximum relative pressure of 0.995 was reached. Adsorption–desorption isotherms were made by recording the increase–decrease of the sample weight at the different relative pressures.

The specific surface area was calculated applying the multi-point BET method [22]. The mesopore size distribution curve was obtained by using the desorption branch of the nitrogen isotherm, according the Orr–Dalla Valle method [23].

X-ray powder diffraction patterns have been carried out with a X-Pert Philips diffractometer using a Cu Kα radiation.

FT IR studies have been performed on pure powder disks of 20–30 mg activated in vacuum at 773 K before any adsorption experiments. A reduction step in hydrogen at the same temperature was carried out before CO adsorption. CO has been adsorbed at 133 K (liquid nitrogen temperature) and spectra have been recorded in the presence of CO and after outgassing upon warming up to room temperature. A Nexus Thermonicolet instrument was used (OMNIC software, DTGS detector, 100 scans). All the spectra in this work are reported in common scale.

UV–vis NIR analysis has been performed using a Jasco V570 instrument, equipped with a DR integration sphere for the analysis of pure catalysts powder. All the spectra have been recorded in air at room temperature.

Temperature programmed reduction tests (TPR) are used to identify and evaluate the reducibility of the various nickel species present on the alumina-supported catalysts. In a typical H_2-TPR test the as-calcined catalyst is reduced by a 10% H_2/Ar gas mixture, while the temperature is ramping up from RT to 1173 K at a rate of 15 °C/min. In cyclic TPR-TPO, upon the first reduction cycle, the sample is first cooled down to room temperature in helium, and eventually oxidized in a 20% O_2/He gas mixture up to 773 K with a ramping rate of 15 °C/min and a 30-min hold at the final temperature. The subsequent TPR cycle is conducted following the same procedure described previously.

2.3. Catalytic experiments

An isothermal tubular quartz flow reactor, containing a fixed bed with 44 mg of catalyst mixed with 440 mg of silica glass particles (60–70 mesh sieved) was fed with 40 Nml/min (GHSV = 54,000 h^{-1}) of a gaseous mixture 39.3% He, 54.6% water, 4.1% ethanol and 2% phenol (mol/mol). For the thermal conversion experiment the bed was constituted by 484 mg of silica glass. A phenol–water–ethanol single phase liquid solution was pumped through a HPLC pump (Shimadzu Corp. LC-D10 AD) in an appropriately heated (583 K) section of the feed line to produce a gas whose composition corresponds to 168 g_{TOT}/Nm³ of ethanol + phenol (84.9 g/Nm³ of phenol), and 439 g/Nm³ water vapor in the He inert carrier. No catalyst pretreatments were performed. Reactor oven temperature was varied from 773 to 1023 K, and vice-versa. The evaluation of activation energies during partial reactants conversion at low temperature 573–773 K allowed us to exclude at least in this temperature region significant diffusion limitations.

In order to reveal conditioning effect catalytic experiments were performed both rising and reducing reaction temperature (773, 873, 973, 1023 K and reverse).

To investigate sulphur poisoning tetrahydrotiophene (C_4H_8S, THT) was used as a contaminant of the feed. In one series of experiments performed at 973 K, 210 ppm of THT were continuously fed with the reactants, by increasing time on stream up to 6 h. In another series of experiments, also performed at 973 K, the effects of two sequential pulses of THT (first 0.011 mol_S/mol_{Ni} and after 0.033 mol_S/mol_{Ni}) and of a further stay on the sulphur-free stream on the catalytic activity of the different catalysts were studied.

Product analysis was performed with a GC/MS (Focus-ISQ Thermoscientific), in order to have a precise identification of the compounds, and with a gas-chromatograph Agilent 4890 equipped with a Varian capillary column "Molsieve 5A/Porabond Q Tandem" and TCD and FID detectors in series. Between the detectors, a nickel catalyst tube was employed to reduce CO and CO_2 to CH_4. The sampling of the outlet vapors was made by injection, using a gas-tight with a nominal volume of 0.25 ml. A sampling injection point at the end of the vaporization zone allowed us to analyse the reagents and to determine that the feed composition was not modified in this section. Hydrogen was detected as a negative peak in the TCD detector signal of the GC and it was also calculated on the basis of the C-product yields. The two measures were confirmed to be in reasonable agreement.

Analyses were performed when apparent steady state conditions was reached, generally in 1 h. Reactants conversion is defined as follows:

$$X_{reactant} = \frac{n_{react.in} - n_{react.out}}{n_{react.in}} \qquad (1)$$

while selectivity to product i is defined as follows:

$$S_i = \frac{n_i}{v_i(n_{react.in} - n_{react.out})} \qquad (2)$$

Table 1
Properties of the catalysts.

Notation and composition	BET surface area (m^2/g_{CAT})	BET surface area (m^2/g_{SUPP})	Total mesopores volume (cm^3/g_{CAT})	Total mesopores volume (cm^3/g_{SUPP})	Mesopore diameter (nm)	Total H$_2$ consumption	
						(μmol/g$_{CAT}$)	molH$_2$/molNi
Ni Ø 5% SiO$_2$-95% Al$_2$O$_3$	172	172	0.49	0.49	10.1	–	–
Ni16 20% NiO/(5% SiO$_2$-95% Al$_2$O$_3$)	137	171	0.35	0.44	9	3090	1.3
NiMg 20% NiO/20% MgO/(5% SiO$_2$-95% Al$_2$O$_3$)	116	193	0.28	0.47	8.9	3244	1.4
BNi 1%H$_3$BO$_3$/20% NiO/(5% SiO$_2$-95% Al$_2$O$_3$)	140	177	0.37	0.47	9.4	2808	1.2
NiB 20% NiO/1%H$_3$BO$_3$/(5% SiO$_2$-95% Al$_2$O$_3$)	138	175	0.38	0.48	9.6	2944	1.3
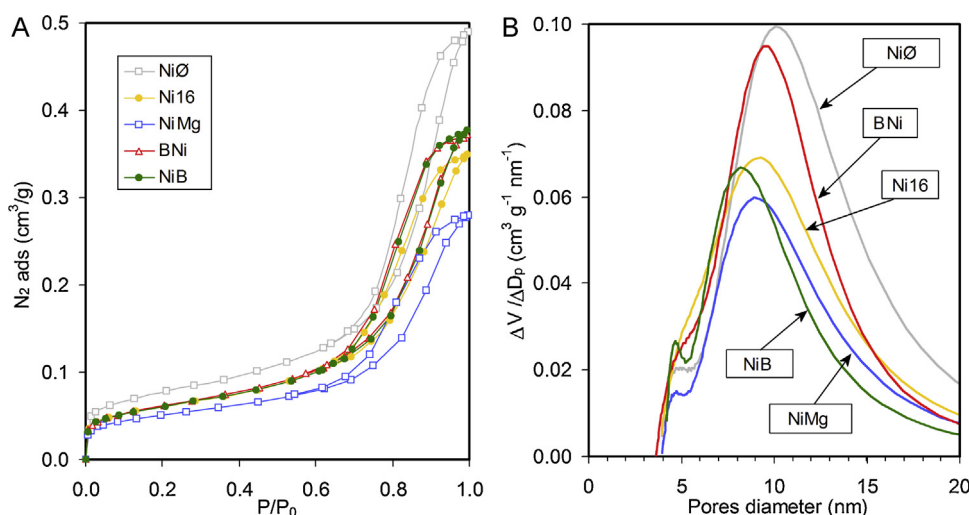
Fig. 1. (A) Typical N$_2$ adsorption–desorption isotherm at 78 K for NiØ, Ni16, NiMg, BNi and NiB, samples; (B) mesopores size distribution for NiØ, Ni16, NiMg, BNi and NiB samples, evaluated from N$_2$ desorption isotherms at 78 K, according the Orr–Dalla Valle method.

where n_i is the number of moles of compound i, and ν_i is the ratio of the stoichiometric reaction coefficients. When applied to the overall carbon feed, n_i is the carbon number of moles of compound i, n_{react} is the carbon number of moles of reactants mixture as a whole and $\nu_i = 1$.

Hydrogen yield is defined as the molar percentage of hydrogen produced with respect to the maximum hydrogen that could be produced (total conversion of both reactants in steam reforming producing 6 H$_2$ molecules for each ethanol molecule and 14 H$_2$ molecule for each phenol molecule).

The results of repeated experiments allowed us to evaluate reproducibility of the order of ±3% (mol/mol).

3. Results and discussion

3.1. Morphology characterization of the fresh catalysts

Fig. 1A shows the adsorption–desorption nitrogen isotherm at 78 K for the four catalyst powders tested and for the Siralox support. All the isotherms can be considered as "IV-type" according the Brunauer classification [24]. The total porosity, evaluated by the maximum value of the ordinate in correspondence of a relative pressure P/P_0 near to the unit, decrease from 0.49 cm^3/g$_{CAT}$ for NiØ to 0.28 cm^3/g$_{CAT}$ for NiMg. The Ni16, BNi and NiB samples on the other hand display almost the same total pores volume (0.35–0.38 cm^3/g$_{CAT}$). Similar trend occurs for the specific surface area, that changes from 172 m^2/g$_{CAT}$ for NiØ to 116 m^2/g$_{CAT}$ for NiMg sample, but it remains around to 138 m^2/g$_{CAT}$ for the other three samples (Table 1).

On the other hand, if the surface area and the porosity are related to the support weight, instead of the overall catalyst weight, it is evident that both surface area and total pore volume values are hardly affected by impregnation. This indicates that a thin layer of the supported phases is mostly formed, decreasing a little bit the diameter of the pores but barely affecting the morphology of the powder. In fact, all samples are characterized by "cylindrical pores" as suggested by the shape of the adsorption–desorption curves [25].
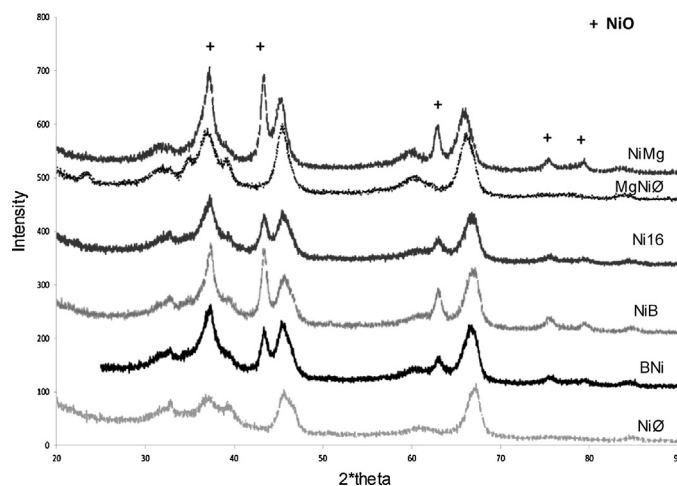
Fig. 2. XRD diffraction patterns of the catalysts, of bare Siralox and of MgO on Siralox (MgNiØ) (Cu Kα radiation).
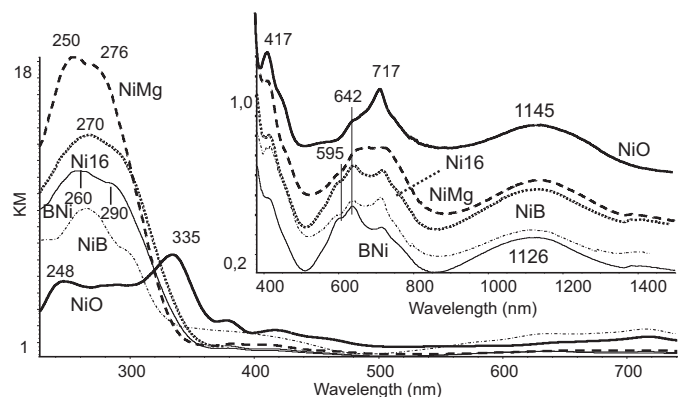
Fig. 3. DR-UV–vis NIR spectra of the catalysts and of pure NiO.

The pore size distribution (Fig. 1B) can be considered unimodal for all the samples. A small decrease of the pore diameter from 10.1 nm, for the NiØ, to around 9 nm both for Ni16 and for NiMg samples, can be observed, whereas both the boron containing samples give almost the same pore diameter (9.5 nm).

3.2. X-Ray diffraction study of the fresh catalysts

XRD pattern of the Siralox support (indicated as NiØ in Fig. 2) can be attributed to a tetragonally distorted defective spinel alumina similar to δ-Al_2O_3 or γ'-Al_2O_3 [26]. This assignment, more than to γ-Al_2O_3 (cubic defective spinel) is due to the partial splitting of the two most intense 440 and 400 spinel peaks (near $2\theta = 67°$ and $46°$). Interestingly, the spectrum of the support MgNiØ does not present additional peaks except for those of the spinel-type phase. However, in this case the tetragonal deformation seems lowered, being that the two 440 and 400 spinel peaks are more symmetric. This suggests an evolution towards the pattern of the stoichiometric cubic spinel $MgAl_2O_4$, possibly associated to a penetration of Mg^{2+} in the alumina lattice. This is contrary to what happens for Ni16, where the presence of NiO peaks and the splitting of the spinel-phase peaks is observed. This indicates a non-significant Ni^{2+} penetration into the lattice, in contrast to what occurs with Mg^{2+} and it is likely associated to the different site coordination preference of the two cations. Ni^{2+} (d^8) definitely prefers octahedral sites, thus $NiAl_2O_4$ is essentially an inverse spinel, while Mg^{2+} (d^0) has no site preference, thus $MgAl_2O_4$ is essentially a normal spinel. The patterns of all other samples, together with the alumina spinel pattern, present the peaks of a rock-salt type phase, i.e. NiO. For the NiMg and NiB samples the NiO signals are equally intense, while for Ni16 and BNi they are weaker. This suggests that both Mg and B species prevent Ni dispersion or Ni penetration in the spinel lattice. The analysis of the crystal size of the nickel oxide phase through the Scherrer calculation gives rise to values lower than 20 nm in all cases. Both specimen NiMg and NiB show peaks sharper than those of the other two samples (Ni16 and BNi), but not more intense than these two samples. This fact is to be related to the slightly larger dimensions of the NiMg and NiB crystallites compared to those of Ni16 and BNi samples.

3.3. DR-UV–vis-NIR spectra of the fresh catalysts

The diffuse reflectance ultraviolet-visible-Near Infrared (DR-UV–vis-NIR) spectra of the Ni16, NiMg, NiB and BNi catalysts are reported in Fig. 3. The pure support does not show any absorption evident at the scale reported in the figure. The sample Ni16 shows a weak broad absorption in the NIR region centered at 1126 nm, and a complex absorption in the visible, with quite sharp maxima at 595, 642, 717 nm. All these features are due to d–d transitions of
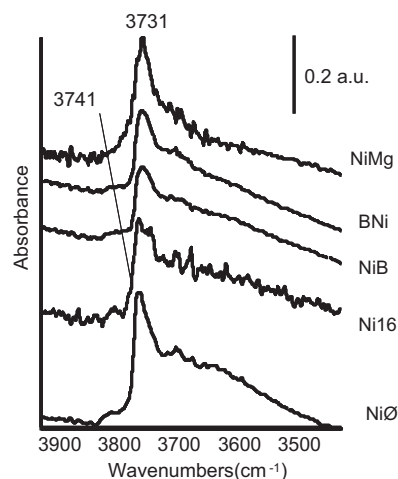

Fig. 4. FT IR spectra of pure powder catalysts and support after outgassing at 500 °C. OH stretching region.

Ni^{2+} cations. As discussed previously [27], this spectrum is nearly the sum of those of bulk NiO and of low loading NiO on Alumina, where only isolated Ni^{2+} cations are observed.

In the UV region a strong band, probably with several components, is observed and a main maximum at 270 nm: this absorption is typically associated to O^{2-} (2p) $\rightarrow$ Ni^{2+} (3d) charge transfer transitions, that gives usually rise on bulk oxides to the band gap transition. The absorption is definitely different here from that of bulk NiO, and it is attributed mostly to NiO nanoparticles and Ni^{2+} cations [27].

The overall UV–vis-NIR spectra of BNi and NiB catalysts are very similar to that of Ni16, while that of NiMg appears to be a little modified in the Vis and NIR region, where the feature at 595 nm, due to a d–d transition of isolated Ni^{2+} cations, disappeared, while the features associated to NiO nanoparticles are perhaps broadened. The absorbance in the UV region is strengthened and slightly shifted to lower wavelength. The UV spectra suggest that Mg^{2+} ions displaces dispersed Ni^{2+} cations, favouring crystallization of NiO particles, in agreement with XRD data and FT IR data discussed below.

3.4. IR characterization of catalysts

The IR spectra in the OH stretching region of the samples under study (Fig. 4) show a slight shift of the main OH stretching band from 3741 cm^{-1} for the support NiØ to 3731 cm^{-1} for NiMg. This
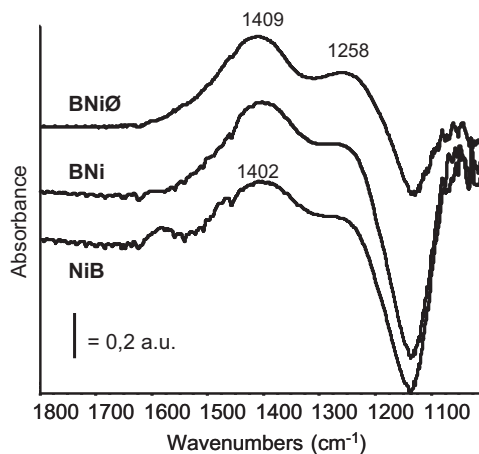

Fig. 5. FT IR subtraction spectra of B-containing pure powder catalysts and support after outgassing at 773 K. Borate stretching region.

band is assigned to the OH stretching mode of surface silanol groups associated to the presence of silica in the support. In the case of MgNiØ and NiMg samples this band can also have a contribution from MgOH groups, which are expected to absorb in the same region. However, the spectrum of activated NiØ shows features at 3790 and near 3775 cm^{-1}, as well as at 3724 cm^{-1}, and at ca 3670 and 3600 cm^{-1}, similar to those present on the spectra of alumina, which are assigned to Al–OH groups. The intensity of these bands decreases in the other samples suggesting that the Al–OH species may be involved in the anchoring of surface species. There were no peaks assigned to new OH groups related to boron or Mg doping, i.e. B–OH and/or mixed B–OH–Al.

Fig. 5 shows the spectra of BNiØ, NiB and BNi samples from which the spectrum of pure support has been subtracted. A main band is detected in the region near 1402–1409 cm^{-1} typically due to the asymmetric stretching of surface trigonal borate anions (BO$_3^{3-}$) in the anhydrous form, which have prevailed after the dehydration of the catalysts at 773 K. Another B–O stretching component at lower frequencies is detected below 1300 cm^{-1}, which can be attributed to the asymmetric BO$_4$ stretching of highly asymmetric tetrahedral borate species [28]. In all cases a negative band is observed at 1130 cm^{-1}, which is assigned to surface Al–O modes perturbed by, or substituted by, the deposition of borate species.

Low temperature CO adsorption has been performed over the catalysts, after a mild reduction treatment in hydrogen, and the resulting spectra are reported in Figs. 6–8.

The spectra of CO adsorbed on the reduced Ni16 catalyst have been extensively discussed previously [27] and are reported in Fig. 6, inset B, for comparison. While the band centered near 2158 cm^{-1} is due to CO hydrogen-bonded on surface OH′ and is very labile, three groups of bands due to chemisorbed CO may be distinguished. The sharp and strong peak whose maximum shifts upwards from ca 2185 cm^{-1} to near 2195 cm^{-1} by decreasing coverage is assigned to CO coordinated over ionic species, i.e. Al ions from the support, and Ni^{2+} ions. Its behaviour towards outgassing upon warming is consistent with the proposed assignation. The band observed at 2098 cm^{-1} at the highest coverage shifting downwards to near 2070 cm^{-1} by decreasing coverage is due to on-top carbonyls on extended but small Ni particles. In fact, the observed shift down is associated to reduced coupling by decreasing coverage typically due to parallel vibrators on extended surfaces. However, on extended Ni particles another band of adsorbed CO is usually also present due to bridging species. The absence of this second band indicates that these particles are indeed very small or characterized by a high content of defect sites (edges, corners). The four bands at 2130, 2060, 2044 and 2020 cm^{-1} disappear in parallel upon outgassing and are consistent with an assignment to weakly adsorbed polycarbonyl species [29] such Ni(CO)$_4$, thus being assumed to provide evidence of reduced isolated Ni centers.

CO adsorption over the NiB catalyst gives rise to the spectra reported in Fig. 6, which are closely similar to those observed on Ni16 (Fig. 6, inset B) and behave in the same way upon decreasing CO coverage. Thus, it is concluded that boron deposition on the support does not affect significantly the morphology and distribution of nickel reduced species at the catalyst surface. On the contrary, while the metal particles are the main species at the Ni16 catalyst surface, the relative intensity of the bands suggest that ionic Nickel species may be more abundant, relatively, on the NiB catalyst surface.

The analysis of the high frequency region of the subtraction spectrum referred to the highest CO coverage (inset A in Fig. 6) shows clearly two negative components at 3736 and 3694 cm^{-1}, the latter corresponding to terminal OH groups on boron, respectively, perturbed by CO adsorption and shifted towards lower frequencies. This is evidence that B–OH species are formed and are able to interact with CO through H-bonds.

The spectra of CO adsorbed on reduced BNi are reported in Fig. 7. Again, the bands of hydrogen-bonded CO (ca. 2160 cm^{-1}, disappearing upon outgassing), of CO adsorbed on ionic centers (2185 shifting to 2195, 2200 cm^{-1}) and on extended Ni particles (2098 cm^{-1} shifting to 2070 cm^{-1}) are observed. The reported shift that these bands undergo at decreasing CO coverage, as discussed for the Ni16 and NiB catalysts spectra, is a further evidence of the exposition of ions (Al^{3+} and Ni^{2+} ions) and metallic nickel particles at the catalyst surface. On the other side, it seems that boron impregnation on Ni species leads to the complete disappearance of the polycarbonyl species in the spectra of adsorbed CO. This effect can be explained considering that boron impregnation, even when performed after the deposition of Ni species, affects mainly the alumina support and the atomically dispersed nickel phase, leaving almost unchanged the small size and more structured exposed metal particles.

CO adsorption over NiMg results in the spectra reported in Fig. 8. As in the previous experiments, the main bands are due to CO interacting with surface OH groups (band at 2155 cm^{-1}, disappearing upon outgassing) and to CO interacting with surface ions (band at 2175 cm^{-1}), still detectable after outgassing. The latter band recorded in the presence of CO at liquid nitrogen temperature is complex and is showing two components at 2182 and 2172 cm^{-1} (see also the corresponding 2nd derivative pattern, overlapped in Fig. 8). The 2172 cm^{-1} component corresponds to a highly unstable carbonyl complex, which disappears immediately after outgassing and its frequency corresponds to the characteristic value reported in the literature for Mg–CO complexes formed in exchanged zeolites. This suggests that Mg^{2+} cations are at least in part exposed at the surface [30]. The bands at lower frequency appear to be significantly different, suggesting a different morphology of the surface nickel particles. The component at 2092 cm^{-1}, as well as the maxima between 2070 and 2020 cm^{-1} disappear immediately after outgassing, leaving a quite broad component at 2080 cm^{-1}, with a shoulder at 2037 cm^{-1}, and another intense and broad band at 1970 cm^{-1}, which has been only detected over this sample, due to bridging carbonyl species. This behaviour points out the progressive disappearance of the atomically dispersed nickel phase during the experiment, and the formation of larger extended nickel particles due to a surface restructuring in the presence of CO. The highly defective metallic nickel particles we observed over the Ni16 samples, characterized by the band at 2098–2070 cm^{-1}, are not evident anymore, whereas a most usual spectrum of CO adsorbed on extended metal particles, with both terminal (2098 cm^{-1}) and bridging (1957 cm^{-1}) carbonyl species points out to the formation of well structured Ni particles exposing flat planes. It can be therefore concluded that Mg addition results in the formation of larger metal particles, as also reported for other supports by Jensen et al. [31].

3.5. TPR results

In Fig. 9 we report the results obtained from TPR studies performed on the as calcined catalysts. The total hydrogen consumption for each catalyst is reported in Table 1. The total consumption of hydrogen is in all cases slightly higher than needed to completely reduce the nickel from the bivalent to the zerovalent state. However, the reduction temperatures measured in the heating condition of TPR (threshold at $T > 673$ K) are higher than those used in static conditions in the pretreatment of IR experiments. These temperatures are also mostly higher than those used in flow catalytic experiments, where catalyst reduction seems to occur at least in part. This suggests that the organics reactant (ethanol and phenol) and/or the CO produced may be more efficient than hydrogen as reducing agents.
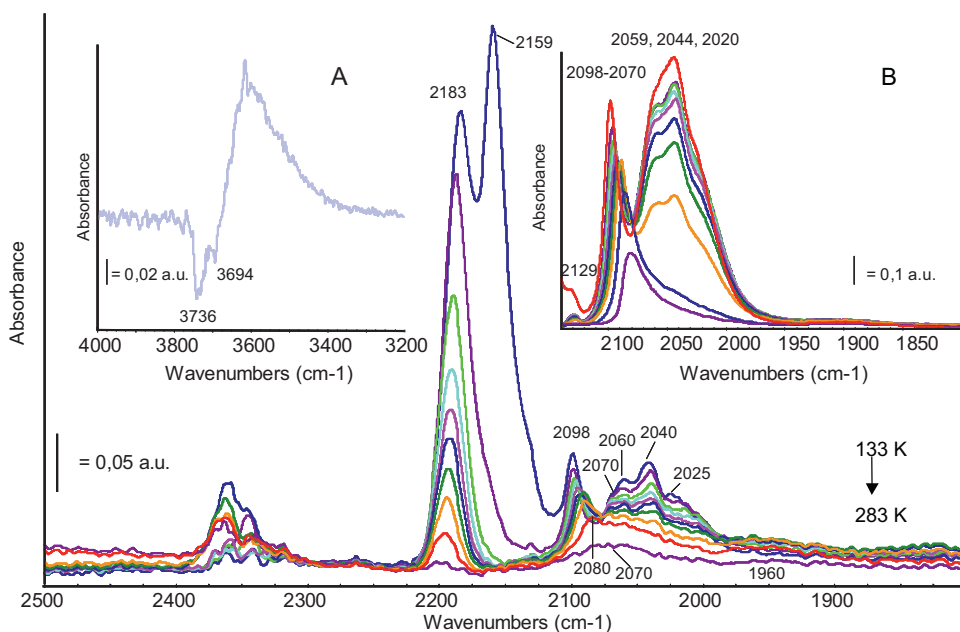
Fig. 6. FT IR spectra of the surface species arising form low temperature CO adsorption over NiB catalyst reduced in hydrogen. Inset A: spectrum of CO adsorption recorded at−413 K: OH stretching region. Inset B: FT IR spectra of the surface species arising form low temperature CO adsorption over Ni16 catalyst reduced in hydrogen. The activated surface has been subtracted.

The TPR profile of the Ni39 sample (prepared in the same way as Ni16 but containing 39% Ni, as described elsewhere [20]), is also reported in Fig. 9 for comparison: it shows an additional reduction peak (not observed in the samples considered here) in the range of 623–673 K, attributed to the reduction of "normal" (unsupported) NiO particles, in agreement with the literature [32–35]. Thus, the TPR spectrum of Ni16 and of the other samples considered here, in spite of the observation of NiO by XRD, does not show the features associated with the reduction of NiO particles. This corroborates with what is observed by the UV (see above) and Raman spectroscopy [19]. From these results, we suggest that, on Ni16 catalyst, particles giving rise to the XRD pattern of NiO but with different electronic properties exist, likely very small nanoparticles strongly

interacting with the support and resistant to reduction. These particles will be defined hereinafter "NiO nanorafts".

All TPR patterns are quite complex and several components could be discriminated and qualitatively discussed (see also peak deconvolution in Figure S1 in Supplementary Data). The fresh Ni16 catalyst shows a main, complex, reduction peak with a maximum at ca. 1010 K, although a shoulder at lower temperature indicates that reduction processes start already just above 773 K. Deconvolution of the main peak results in the detection of three reduction components we related to the reduction of three different Nickel ion species at the surface. A possible interpretation is associated to the results of IR experiments discussed above: the three species are identified as isolated reduced Ni species (forming polycarbonyls
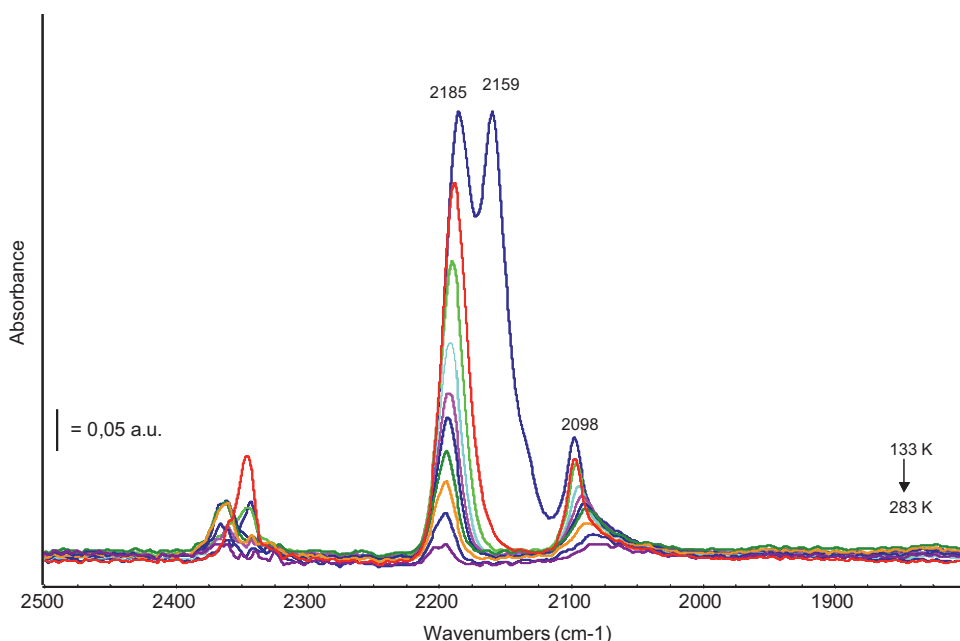

Fig. 7. FT IR spectra of the surface species arising from low temperature CO adsorption over BNi catalyst reduced in hydrogen. The activated surface has been subtracted.
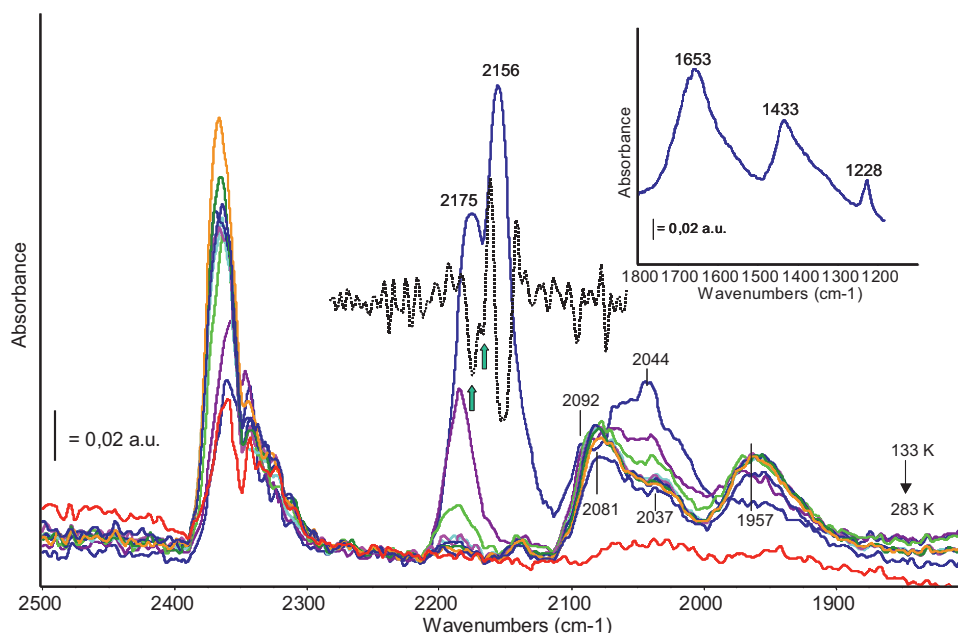
Fig. 8. FT IR spectra of the surface species arising from low temperature CO adsorption over NiMg catalyst reduced in hydrogen. Broken line: 2nd derivative. Inset: spectrum of CO adsorption recorded at 133 K: low frequency region. The activated surface has been subtracted.

with CO), small Ni metal particles, and isolated unreduced Ni ions. The three TPR components observed for Ni16 can be thus assigned to the formation of these three species. Thus, the low temperature reduction shoulder is assigned to very small NiO nanorafts which upon reduction produce isolated reduced Ni species (species I). The main peak is attributed to larger NiO nanorafts which lead to small Ni particles (species II). The high temperature component is associated to the reduction of dispersed Ni^{2+}, the most resistant to reduction (species III).

As for sample NiMg, the TPR curve shows the same three components and the comparison with results reported for Ni16 catalysts shows that the addition of Mg causes a small shift of the main reduction peak toward lower temperatures, corresponding to an increase of the reducibility of species I and II. Apparently a slight increase of the total amount of NiO nanorafts species II (in agreement with XRD) is also detected (broad reduction peak). The TPR curves for NiB can be discussed accordingly. Focusing on the low

temperature components, the total amount of species I and II is increased in comparison with Ni16, in agreement with XRD, but the reducibility is almost not affected. The same interpretation can be more difficult for BNi sample, where the low temperature shoulder in the TPD curve seems to be slightly decreased in intensity compared to sample Ni16, in agreement with IR data showing the full disappearance of isolated reduced Ni.

3.6. Catalytic behaviour in sulphur free conditions

As reported elsewhere [19] in the blank reaction test the conversion of reactants is very small at 773–973 K and still largely partial at 1023 K with mainly production of ethylene and acetaldehyde. Over the Ni16 catalyst (Table 2) in the increasing temperature experiment, no steam reforming activity is observed at 773 K, although ethanol is almost completely converted The main products are: ethylene (46% of carbon selectivity): phenol ethylation products (36% of carbon selectivity), acetaldehyde (11% of carbon selectivity) and dialkylates (5% of carbon selectivity). At 873 K phenol conversion remains small. There is a little selectivity toward CO and CO_2 (9% and 13% on carbon basis, respectively) but the main products remain ethylene (selectivity 40%), monoalkylate products (selectivity 14%), acetaldehyde (selectivity 13%) and ethane (selectivity 10%). At 973 and 1023 K the picture changes completely; it is achieved complete conversion of both reactants in steam reforming activity to CO and CO_2 as main products, both in the increasing and decreasing temperature mode, accompanied by a hydrogen yield ranging around 80–82%.

In the decreasing T experiments a conditioning effect of the catalyst is observed. In fact at 873 K complete conversion of ethanol and 90% conversion of phenol occur, the main products being steam reforming products (CO_2 57%, CO 27%). Small amount of ethylene and ethane are also found. After a further reduction of the reaction temperature down to 773 K, the steam reforming activity almost vanishes: the conversions are almost similar to those obtained in the increasing temperature experiment but in this case CO_2 is the more abundant product with 62% selectivity, whereas ethylene, CO (selectivity 5%), dialkylates (selectivity 10%) ethane (selectivity 2%) and methane (selectivity 2%) are also observed.
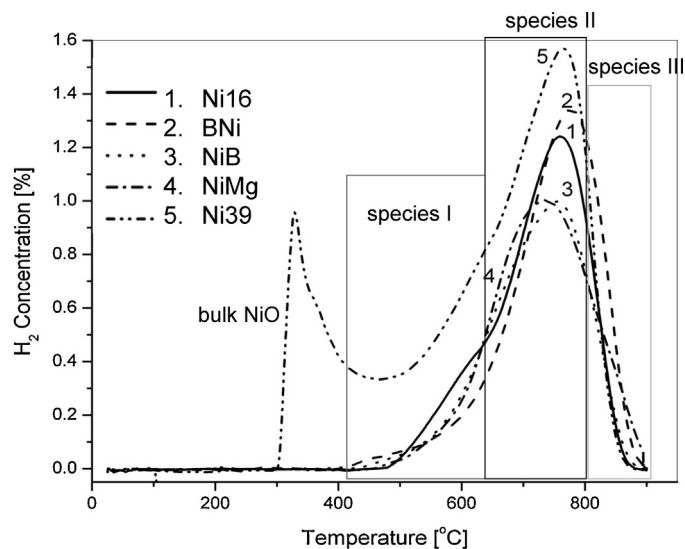

Fig. 9. H_2-TPR analysis of the Ni-based catalysts.

Table 2
Carbon and reactants conversions (Xi) and carbon-based selectivities to products (Si) on phenol–ethanol–water reaction on Ni16 catalyst.

Increasing temperature experiment on Ni16

T furnace [K]	C conversion	X C_2H_6O	X C_6H_6O	X H_2O	Y H_2
773 K	0.55	0.98	0.27	−0.05	0.02
873 K	0.55	0.86	0.25	−0.01	0.06
973 K	0.95	0.98	0.93	0.46	0.80
1023 K	0.99	1.00	0.98	0.46	0.82

T furnace [K]	S CH_4	S CO	S CO_2	S CH_2CH_2	S CH_3CH_3	S CH_3OH	S CH_3CHO	S C_6H_6	S C_8	S C_{10}
773 K	0.00	0.00	0.01	0.46	0.00	0.01	0.11	0.00	0.36	0.05
873 K	0.01	0.09	0.13	0.40	0.10	0.00	0.13	0.01	0.14	0.00
973 K	0.01	0.36	0.59	0.00	0.00	0.00	0.03	0.00	0.00	0.00
1023 K	0.00	0.43	0.56	0.00	0.00	0.00	0.00	0.00	0.00	0.00

Decreasing temperature experiment on Ni16

T furnace [K]	C conversion	X C_2H_6O	X C_6H_6O	X H_2O	Y H_2
1023 K	1.00	1.00	1.00	0.00	0.77
973 K	1.00	0.96	1.00	0.00	0.83
873 K	0.94	1.00	0.90	0.00	0.66
773 K	0.51	0.98	0.20	0.00	0.37

T furnace [K]	S CH_4	S CO	S CO_2	S CH_2CH2	S CH_3CH_3	S CH_3CHO	S C_6H_6	S C_8	S C_{10}
1023 K	0.00	0.60	0.39	0.00	0.00	0.00	0.00	0.00	0.00
973 K	0.02	0.39	0.59	0.00	0.00	0.00	0.00	0.00	0.00
873 K	0.05	0.27	0.57	0.05	0.04	0.00	0.02	0.01	0.00
773 K	0.02	0.05	0.62	0.14	0.02	0.03	0.02	0.00	0.10

In Table 3 the catalytic results obtained on BNi are reported. In the increasing temperature experiment the results are similar to those observed on Ni16. The catalyst is even more active in converting ethanol to ethylene but less active in phenol ethylation at 773 and 873 K. The steam reforming activity is complete at 973 and 1023 K. By reducing the reaction temperature, steam reforming of ethanol still occurs at 873 K, while steam reforming of phenol is strongly reduced. In any case, the activity at 873 K in the reducing temperature experiment is different with respect to that observed in the increasing temperature experiment, showing also in this case a conditioning effect. Again at 773 K alkylation and ethanol

dehydration and dehydrogenation activities reappear but steam reforming is not completely suppressed. In practice, the BNi catalyst is slightly less active than Ni16 as a steam reforming catalyst at 873 K after conditioning, while both show complete conversion activity at 973 and 1073 K.

The NiB catalyst, instead, appears to be definitely less active than the previous ones (Table 4). In fact the conversion of phenol is very low also at 973 K, when ethylene and acetaldehyde are still produced with significant selectivities from ethanol. Steam reforming occurs with complete conversion only at 1023 K. Also in the reducing temperature experiments at 973 and 773 K the NiB

Table 3
Carbon and reactants conversions (Xi) and carbon-based selectivities to products (Si) on phenol–ethanol–water reaction on BNi catalyst.

Increasing temperature experiment on BNi

T furnace [K]	C conversion	X C_2H_6O	X C_6H_6O	X H_2O	Y H_2
773 K	0.62	0.97	0.14	−0.08	0.00
873 K	0.59	0.87	0.07	−0.03	0.04
973 K	0.95	1.00	0.92	0.50	0.85
1023 K	0.98	1.00	0.96	0.48	0.84

T furnace [K]	S CH_4	S CO	S CO_2	S CH_2CH_2	S CH_3CH_3	S CH_3CHO	S CH_3COCH_3	S C_6H_6	S C_7	S C_8	S C_{10}
773 K	0.00	0.00	0.03	0.65	0.01	0.19	0.01	0.00	0.00	0.01	0.09
873 K	0.02	0.04	0.08	0.52	0.05	0.23	0.00	0.01	0.02	0.00	0.02
973 K	0.00	0.28	0.72	0.00	0.00	0.00	0.00	0.00	0.00	0.00	0.00
1023 K	0.00	0.35	0.65	0.00	0.00	0.00	0.00	0.00	0.00	0.00	0.00

Decreasing temperature on BNi

T furnace [K]	C conversion	X C_2H_6O	X C_6H_6O	X H_2O	Y H_2
1023 K	1.00	1.00	1.00	0.47	0.83
973 K	1.00	1.00	1.00	0.50	0.86
873 K	0.66	0.93	0.48	0.27	0.51
773 K	0.54	0.95	0.26	0.06	0.18

T furnace [K]	S CH_4	S CO	S CO_2	S CH_2CH_2	S CH_3CH_3	S CH_3CHO	S C_6H_6	S C_8
1023 K	0.00	0.44	0.56	0.00	0.00	0.00	0.00	0.00
973 K	0.00	0.34	0.65	0.00	0.00	0.00	0.00	0.00
873 K	0.05	0.36	0.55	0.01	0.02	0.00	0.01	0.00
773 K	0.02	0.03	0.35	0.29	0.03	0.11	0.00	0.18

Table 4
Carbon and reactants conversions (Xi) and carbon-based selectivities to products (Si) on phenol–ethanol–water reaction on NiB catalyst.

Increasing temperature experiment on NiB

T furnace [K]	C conversion	X C_2H_6O	X C_6H_6O	X H_2O	Y H_2
773 K	0.65	1.00	0.21	−0.07	0.00
873 K	0.33	0.71	0.00	−0.03	0.03
973 K	0.38	0.67	0.19	0.08	0.20
1023 K	0.99	1.00	0.99	0.44	0.80

T furnace [K]	S CH_4	S CO	S CO_2	S CH_2CH_2	S CH_3CH_3	S CH_3CHO	S CH_3COCH_3	S $(CH_3CH_2)_2O$	S C_6H_6	S C_8	S C_{10}
773 K	0.00	0.01	0.02	0.59	0.02	0.17	0.01	0.00	0.00	0.15	0.04
873 K	0.01	0.02	0.03	0.72	0.01	0.20	0.00	0.00	0.00	0.00	0.00
973 K	0.05	0.34	0.28	0.16	0.00	0.11	0.01	0.00	0.05	0.00	0.00
1023 K	0.00	0.50	0.50	0.00	0.00	0.00	0.00	0.00	0.00	0.00	0.00

Decreasing temperature experiment on NiB

T furnace [K]	C conversion	X C_2H_6O	X C_6H_6O	X H_2O	Y H_2
1023 K	1.00	1.00	1.00	0.46	0.82
973 K	0.79	1.00	0.66	0.15	0.32
873 K	0.71	0.86	0.57	0.13	0.25
773 K	0.18	0.42	0.02	0.04	0.11

T furnace [K]	S CH_4	S CO	S CO_2	S CH_2CH_2	S CH_3CH_3	S CH_3CHO	S CH_3COCH_3	S $(CH_3CH_2)_2O$	S C_6H_6	S C_8	S C_{10}
1023 K	0.00	0.47	0.53	0.00	0.00	0.00	0.00	0.00	0.00	0.00	0.00
973 K	0.03	0.28	0.28	0.27	0.06	0.04	0.00	0.00	0.02	0.02	0.00
873 K	0.01	0.09	0.29	0.48	0.02	0.05	0.02	0.00	0.01	0.04	0.00
773 K	0.01	0.06	0.45	0.22	0.00	0.09	0.03	0.05	0.00	0.10	0.00

catalyst performs worst than the Ni16 and BNi as a steam reforming catalyst.

The catalytic data obtained on NiMg catalyst are reported in Table 5. At 773 K ethanol is converted to acetaldehyde, ethylene, acetone, diethylether, acetic acid, while phenol and ethanol are also converted to monoalkylation products. However, some steam reforming activity to CO_2 and CO is already observed. Steam reforming activity is complete starting from 973 K, it is maintained at this level also at 873 K and is still evident at 773 K in the reducing temperature experiments. The data suggest that NiMg is a better steam reforming catalyst than Ni16 in sulphur-free flows.

3.7. Catalytic behavior under 210 ppm of THT

Experiments of steam reforming of ethanol and phenol mixture in the presence of 210 ppm of THT at 973 K have been done with the Ni16, BNi and NiMg catalysts. This experiment has not been performed with NiB because this catalyst at this temperature was

Table 5
Carbon and reactants conversions (Xi) and carbon-based selectivities to products (Si) on phenol–ethanol–water reaction on NiMg catalyst.

Increasing temperature experiments on NiMg

T furnace [K]	C conversion	X C_2H_6O	X C_6H_6O	X H_2O	Y H_2
773	0.61	0.90	0.32	0.00	0.08
873	0.57	1.00	0.28	0.03	0.12
973	1.00	1.00	1.00	0.52	0.88
1023	1.00	1.00	1.00	0.48	0.85

T furnace [K]	S CH_4	S CO	S CO_2	S CH_2CH_2	S CH_3CH_3	S CH_3CHO	S CH_3COCH_3	S $(C_2H_5)_2O$	S CH_3COOH	S C_6H_6	S C_8
773	0.01	0.01	0.06	0. .21	0.00	0.38	0.05	0.01	0.01	0.00	0.25
873	0.05	0.11	0.13	0.30	0.03	0.28	0.03	0.00	0.00	0.02	0.06
973	0.00	0.29	0.70	0.00	0.00	0.00	0.00	0.00	0.00	0.00	0.00
1023	0.00	0.39	0.61	0.00	0.00	0.00	0.00	0.00	0.00	0.00	0.00

Decreasing temperature experiments on NiMg

T furnace [K]	C conversion	X C_2H_6O	X C_6H_6O	X H_2O	Y H_2
1023	1.00	1.00	1.00	0.49	0.85
973	1.00	1.00	1.00	0.50	0.86
873	1.00	1.00	1.00	0.52	0.84
773	0.66	0.99	0.44	0.10	0.23

T furnace [K]	S CH_4	S CO	S CO_2	S CH_2CH_2	S CH_3CH_3	S CH_3CHO	S C_6H_6	S C_8	S C_{10}
1023	0.00	0.38	0.62	0.00	0.00	0.00	0.00	0.00	0.00
973	0.01	0.33	0.67	0.00	0.00	0.00	0.00	0.00	0.00
873	0.05	0.21	0.74	0.00	0.00	0.00	0.00	0.00	0.00
773	0.02	0.05	0.33	0.31	0.04	0.05	0.01	0.17	0.03

Table 6

Carbon and reactants conversions (Xi) and carbon based selectivities to products (Si) on phenol–ethanol–water reaction on Ni16 catalyst under 210 ppm of THT. Reaction conditions: THT, 210 ppm; temperature. 973 K.

Ni16 under 210 ppm of THT													
Time	C conversion	X C_2H_6O	X C_6H_6O	X H_2O	Y H_2	S CH_4	S CO	S CO_2	S CH_2CH_2	S CH_3CH_3	S CH_3OH	S CH_3CHO	S C_6H_6	S C_8
0 min	1.00	1.00	1.00	0.50	0.86	0.01	0.33	0.66	0.00	0.00	0.00	0.00	0.00	0.00
90 min	1.00	1.00	1.00	0.46	0.82	0.01	0.44	0.55	0.00	0.00	0.00	0.00	0.00	0.00
192 min	1.00	1.00	1.00	0.46	0.82	0.01	0.43	0.56	0.00	0.00	0.00	0.00	0.00	0.00
292 min	0.69	1.00	0.48	−0.02	0.07	0.03	0.15	0.05	0.42	0.04	0.02	0.04	0.09	0.18
384 min	0.56	0.90	0.33	0.03	0.12	0.12	0.19	0.12	0.21	0.02	0.00	0.10	0.07	0.17

poorly active toward steam reforming even without sulphur in the feed.

In Table 6 we report the results obtained on Ni16. The data at $t = 0$ are those obtained in the absence of THT, as described in the experimental section. Steam reforming of reactants is complete, CO_2 is the main product with 66% selectivity, CO accounts for 33% selectivity and 15% methane selectivity was also found. At $t = 90$ and $t = 192$ we have almost the same situation even if the selectivity to CO_2 is a little bit lower than before. 292 min after the introduction of THT in the feed, ethanol conversion is still complete while phenol conversion drops to 48%. A different products distribution is now observed, with ethylene becoming the most abundant product with 42% selectivity, with the presence of ethane, acetaldehyde (4% carbon selectivity), benzene (9% carbon selectivity) and monoalkylate phenol (18% carbon selectivity). Steam reforming activity is strongly reduced, with 15% selectivity to CO and 5% to CO_2 while methane selectivity is 3%. At 384 min on stream we have a further decrease in the conversions of both reactants to 90% for ethanol and 33% for phenol but steam reforming product selectivity does not decrease further.

On BNi, in the absence of sulphur we observe almost total conversion to steam reforming products, but small additional production of methane, ethylene and benzene that decrease hydrogen yield to 0.73 (Table 7). As in the previous case, any remarkable change is observed before 192 min and this is related to the transient to feed the THT to the catalytic bed. At 292 min we have a complete conversion of ethanol but phenol conversion decreases down to 91%, while the main product became ethylene with 44% carbon selectivity. Steam reforming products are still observed with lower selectivities, CO_2 (14%), CO (16%) and methane (9%), together with acetaldehyde and benzene as minor byproducts. As expected, further deactivation is observed with increased permanence on the sulphur stream: in particular ethanol and phenol conversions decrease to 91% and 27%, respectively. The main product is CO (26%), followed by CO_2 (24%), ethylene (20%), methane (11%), benzene, methanol, acetaldehyde, ethane and monoalkylphenols as minor byproducts. The comparison of the data for Ni16 and BNi obtained at 973 K indicate that Ni16 is a better steam reforming catalyst at this temperature. Both catalysts are severely deactivated in the presence of sulphur, but the presence of boron in BNi slightly improves its sulphur resistance. In Table 8 the results obtained on NiMg are reported. At $t = 0$, $t = 90$ and $t = 192$ min complete steam reforming conversion is observed. At 292 min we have a drop of

the conversion of both ethanol and phenol down to 92% and 16%, respectively. The steam reforming activity is almost completely inhibited and the main product became ethylene (40% selectivity) with several byproducts as monoalkylate (C8 alkylate 25% selectivity), acetaldehyde (15% selectivity), CH_4, ethane and benzene. By increasing the time on stream to 384 min we have a further significant reduction of the conversion to 65% for ethanol and 4% for phenol, with ethylene and acetaldehyde being the main products in the presence of CO and CO_2 and small amounts of benzene and methane. The poisoning effect on NiMg is even stronger than on Ni16.

3.8. Catalytic activity under THT pulses

Activity tests feeding pulses of THT have been performed over the same catalysts. The addition of 0.011 mol_S/mol_{Ni} (corresponding to 36.3 μg_S) to the normal feed (performed 30 min before the product analysis) does not cause significant changes to the catalytic behaviour of the Ni16 catalyst (Fig. 10B). The further addition of 0.033 mol_S/mol_{Ni}, i.e. 109 μg_S, causes an evident deactivation of Ni16 catalyst. Phenol conversion drops to 19%, CO is produced more than CO_2 (in contrast to what was occurring before sulphur addition) and ethylene is the main product of ethanol conversion, together with acetaldehyde and methane (Fig. 10C). With further stay on sulphur free stream, recovery of the full conversion of both reactants through SR is observed (Fig. 10D). CO is produced more than CO_2 and methane is produced in higher amount than usual (10% carbon selectivity).

The first pulse of THT 0.011 mol_S/mol_{Ni} (performed 30 min before the product analysis) causes small changes in the catalytic activity of BNi: ethanol conversion decreases to 94% while phenol conversion decreases to 97% (Fig. 11B). The products distribution also changes with CO_2 being the main product with 39% carbon selectivity, and CO and CH_4 with 16% and 15% selectivity respectively. Addition of the second dose of sulphur does not further impact the product distribution but, surprisingly, it causes an increase of the reactants conversions (Fig. 11C). Once again, permanence in the sulphur free stream leads to the complete recovery of the steam reforming activity already after 135 min. In this case we do not observe any inversion in the CO and CO_2 ratio, in contrast with what is observed on the Ni16 (Fig. 11D and E).

On NiMg the first pulse does not affect the catalytic activity (Fig. 12B) but with the second pulse we have a significant change

Table 7

Carbon and reactants conversions (Xi) and carbon based selectivities to products (Si) on phenol–ethanol–water reaction on BNi catalyst under 210 ppm of THT. Reaction conditions: THT, 210 ppm; temperature 973 K.

BNi under 210 ppm THT													
Time	C conversion	X C_2H_6O	X C_6H_6O	X H_2O	Y H_2	S CH_4	S CO	S CO_2	S CH_2CH_2	S CH_3CH_3	S CH_3OH	S CH_3CHO	S C_6H_6	S C_8
0 min	0.99	0.98	1.00	0.44	0.73	0.06	0.30	0.59	0.03	0.00	0.00	0.00	0.01	0.00
90 min	1.00	1.00	1.00	0.45	0.77	0.05	0.32	0.60	0.01	0.01	0.00	0.00	0.00	0.00
190 min	1.00	1.00	1.00	0.39	0.70	0.06	0.53	0.41	0.00	0.00	0.00	0.00	0.00	0.00
298 min	0.97	1.00	0.91	0.13	0.27	0.09	0.16	0.14	0.44	0.03	0.00	0.06	0.08	0.00
388 min	0.53	0.91	0.27	0.07	0.17	0.11	0.26	0.24	0.20	0.01	0.04	0.04	0.10	0.01

Table 8
Carbon and reactants conversions (Xi) and carbon based selectivities to products (Si) on phenol–ethanol–water reaction on NiMg catalyst under 210 ppm of THT. Reaction conditions: THT, 210 ppm; temperature 973 K.

NiMg under 210 ppm of THT														
Time	C conversion	X C_2H_6O	X C_6H_{60}	X H_2O	Y H_2	S CH_4	S CO	S CO_2	S CH_2CH_2	S CH_3CH_3	S CH_3OH	S CH_3CHO	S C_6H_6	S C_8
0 min	1.00	1.00	1.00	0.52	0.88	0.01	0.29	0.71	0.00	0.00	0.00	0.00	0.00	0.00
90 min	1.00	1.00	1.00	0.46	0.81	0.02	0.43	0.55	0.00	0.00	0.00	0.00	0.00	0.00
192 min	1.00	1.00	1.00	0.51	0.87	0.01	0.32	0.67	0.00	0.00	0.00	0.00	0.00	0.00
292 min	0.44	0.92	0.16	−0.02	0.06	0.03	0.07	0.06	0.40	0.02	0.02	0.15	0.03	0.25
384 min	0.28	0.65	0.04	0.00	0.11	0.11	0.21	0.19	0.21	0.00	0.00	0.20	0.08	0.00
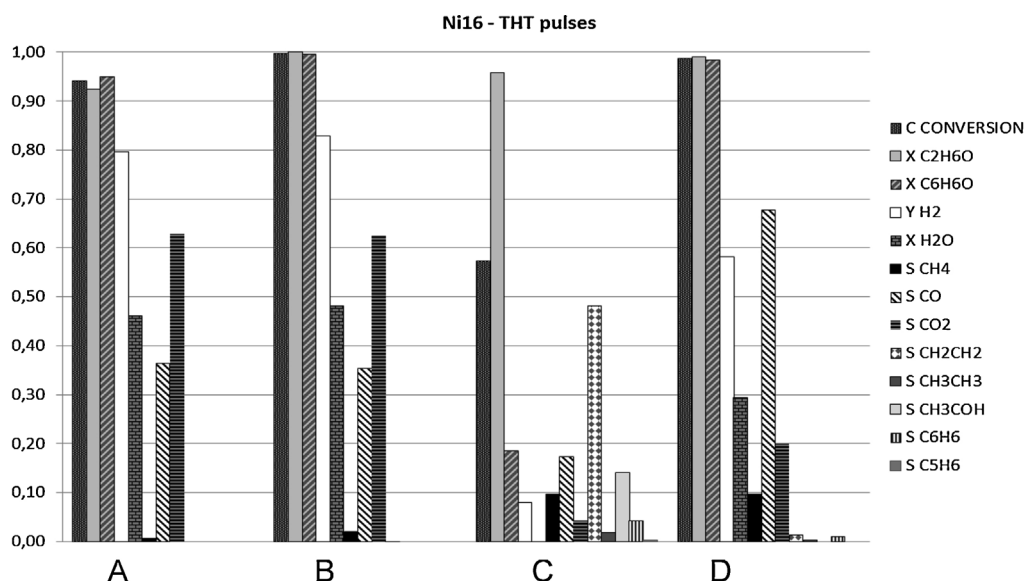
Fig. 10. Reactants conversions and selectivities to products upon pulse sulphur addition experiments on Ni16 catalyst. (A) No sulphur, (B) after 30 min from injection of 0.011 mol_S/mol_{Ni}, (C) after 30 min from injection of 0.033 mol_S/mol_{Ni} and (D) after 135 min.

in the reactants conversions; ethanol conversion is reduced to 94% and phenol conversion decreases to 36% (Fig. 12C). In this case the main product becomes ethylene while acetaldehyde, CO, CO_2 and methane are detected as by products. The catalyst does not recover its activity after 135 min on sulphur free stream after 135 min but on the contrary we observe significant deactivation even if we have a slightly more pronounced activity toward reforming (48% selectivity on carbon basis to CO and 22% CO_2, Fig. 12D). With additional time in the sulphur free stream we recover the complete conversion of ethanol but not that for phenol which is now converted at 84%. In
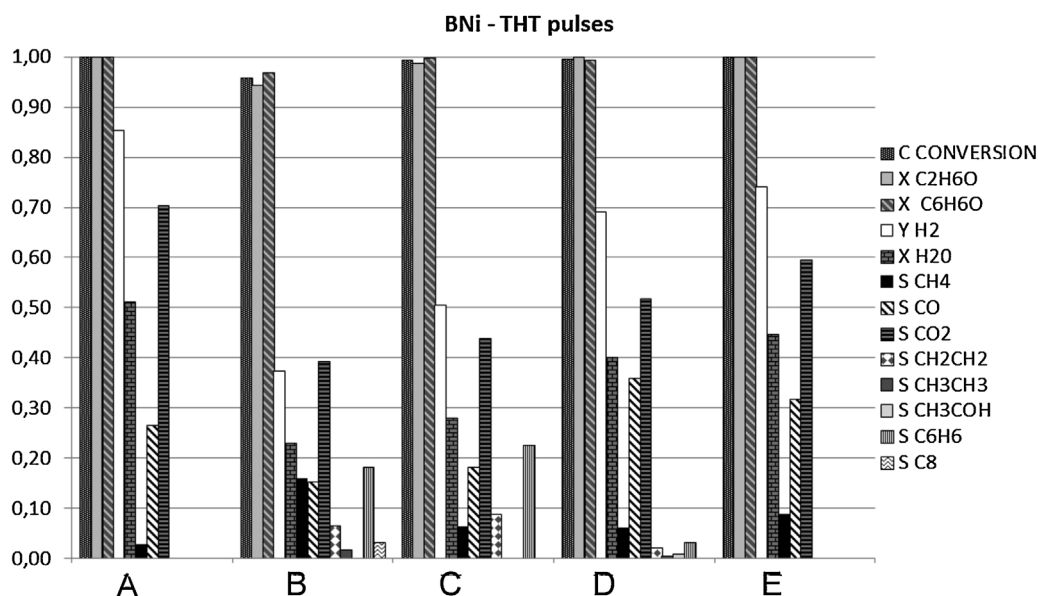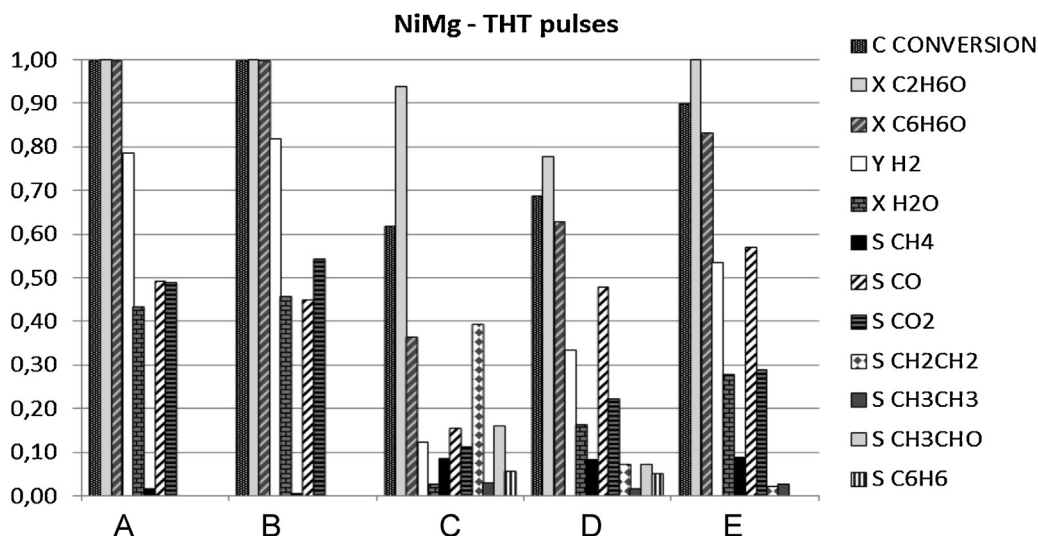

Fig. 11. Reactants conversions and selectivities to products upon pulse sulphur addition experiments on BNi catalyst. (A) No sulphur, (B) after 30 min from injection of 0.011 mol_S/mol_{Ni}, (C) after 30 min from injection of 0.033 mol_S/mol_{Ni}, (D) after 135 min and (E) after 212 min.

Fig. 12. Reactants conversions and selectivities to products upon pulse sulphur addition experiments on NiMg catalyst. (A) No sulphur, (B) after 30 min from injection of 0.011 mol_S/mol_{Ni}, (C) after 30 min from injection of 0.033 mol_S/mol_{Ni}, (D) after 135 min, (E) after 212 min.

this case the main product is CO (57% carbon selectivity) and CO_2 (29% carbon selectivity, Fig. 12E). Thus there is almost complete recovery of the reforming activity with only a little production of CH_4 but with the inversion of CO_2/CO ratio already observed for Ni16.

3.9. IR studies of adsorption of water and phenol

To have some more mechanistic information, we studied the adsorption of the reactants over the catalysts by IR spectroscopy. We report here only data obtained for the best modified Ni-based catalysts. Over NiMg and BNi catalysts, the adsorption of water causes the formation of a broad IR absorption in the region 3600–2400 cm^{-1}, certainly due to H-bonded hydroxyl groups (Fig. 13). The spectra are, however, very different. The spectrum of BNi shows the OH stretching band relative well defined and centered near 3430 cm^{-1} in the first spectrum, shifting progressively up 3550 cm^{-1} before it fully disappears. However, it is to be noted that the first spectrum has been recorded upon outgassing, and the IR spectra recorded at lower frequency show that in all cases

molecular water is no more present. In contrast, the spectrum of NiMg at higher coverage shows a much broader absorption centered near 2900 cm^{-1}, which corresponds to a band at 1645 cm^{-1} due to the vibrational scissoring mode of water (low frequency region of the spectra, not shown here). These features disappear only after outgassing above 423 K. This suggests that on NiMg strongly adsorbed non-dissociated water molecules can be formed while on BNi adsorbed water is more easily fully dissociated.

The surface species detected over the best catalyst, NiMg, after adsorption of phenol are reported in Fig. 14. The spectra are interpreted in agreement with previous studies of IR spectra of phenol [36] and of phenol adsorbed on oxide catalysts [37] including alumina [38]. After contact at r.t. the spectrum seems to be dominated by the features of phenate species (1598 cm^{-1}, 8a ring vibration, 1495 cm^{-1}, 19a ring vibration, 1247 cm^{-1} C–O stretching), but with copresence of un-dissociated phenol (1475 cm^{-1}, 19a ring vibration, 1389 cm^{-1}, broad, in-plane OH deformation). At higher temperature, non-dissociated phenol disappears, while the C–O stretching of phenate species shifts to 1260 cm^{-1}. These band decreases in intensity, likely due to phenol desorption. The
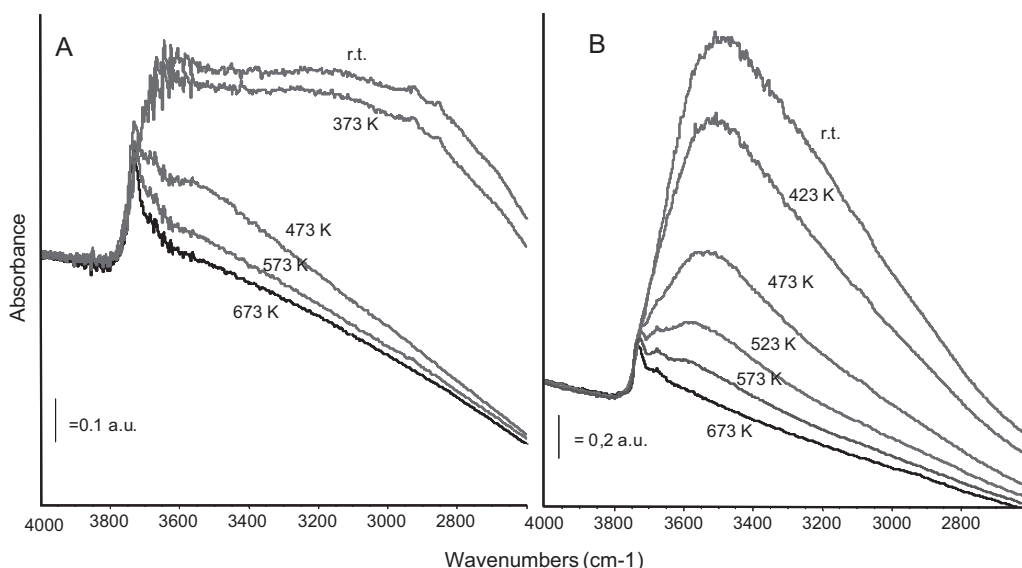

Fig. 13. FT IR spectra of the surface species arising from water vapor desorption over NiMg catalyst (A) and over BNi catalyst (B) after heating at increasing temperatures.
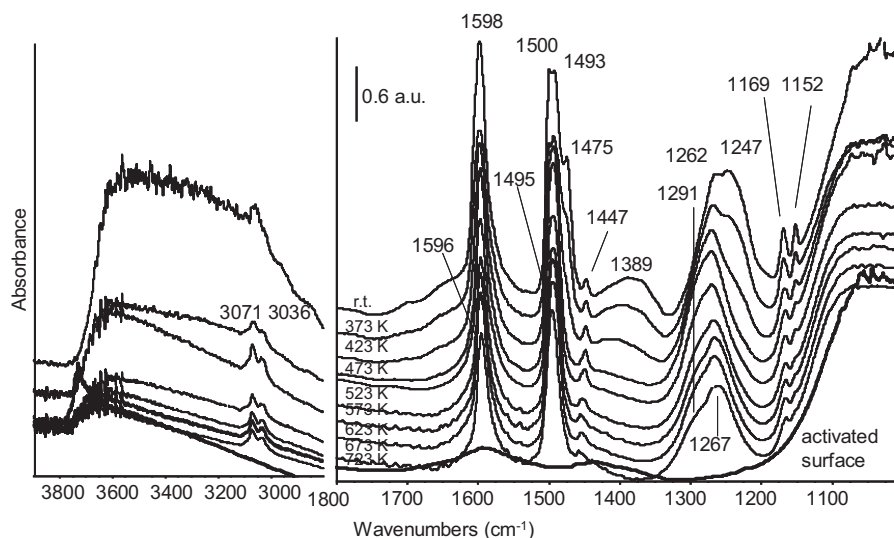
Fig. 14. FT IR spectra of the surface species arising from phenol adsorption over NiMg catalyst after heating at increasing temperatures.

spectrum significantly changes above 473 K, and, particularly in the low frequency region, it becomes more similar to that reported for phenol adsorption on alumina [38] where two types of phenate species were found, terminal, and bridging. The main band at 1267 with shoulder at 1291 cm^{-1} is assigned to CO stretching of terminal phenates on alumina, while the broader component at lower frequency (1250–1165 cm^{-1}) should contain the CO stretching of bridging phenates. The very broad absorption that is observed even at 873 K in the range 1300–1150 cm^{-1} and the persistence of the two bands near 1596 and 1495 cm^{-1}, suggest that very stable aromatic oxygenated species which are refractory to steam reforming form, most likely over the alumina surface. On the contrary, the active adsorbed species for steam reforming are likely phenate species interacting with Ni species, supposed to be responsible for CO stretching at 1260 cm^{-1}, i.e. the most evident species until 723 K.

Very similar species are formed by phenol adsorption over the Boron-modified catalysts (Figures S2 and S3 Supplementary Information).

Summarizing, the IR study of phenol steam reforming suggests that the reaction occurs at the expense of surface phenate species adsorbed on Ni centers. These species start to be reactive above 673 K in the presence of water giving rise to CO and hydrogen. No evidence is found for intermediates or by-products from this reaction. Phenate species on alumina appear to be inactive spectators, while traces of carboxylate species are only found at very high temperature, possibly being also located on alumina and inactive in the reaction. On the other hand, a key factor in the steam reforming catalysis may be associated with the adsorption and activation of water, that give rise to different spectra in the different catalysts.

4. Conclusions

As reported and discussed previously [20], Ni/Al$_2$O$_3$ catalyst with a partial coverage of a theoretical monolayer of NiO is an active steam reforming catalyst, if conditioned, for phenol and ethanol mixture at 873 K, and above.

The effect of the B and Mg addition can be best evaluated considering the behaviour of the catalysts at 873 K in decreasing temperature mode, i.e. after "conditioning" in the reaction medium at higher temperature up to 1023 K. In these conditions NiMg is the best catalyst with total conversion to steam reforming products and small amounts of methane, and hydrogen yield 0.84.

The Mg-free and B-free Ni16 catalyst, under the same conditions, shows incomplete conversion and small production of ethylene, ethane and benzene, together with a predominant steam reforming activity. The sample BNi shows even lower conversion, but a largely predominant steam reforming activity. Instead the catalyst NiB shows, under these conditions, similar conversions to the BNi, but a predominant dehydrating activity towards ethanol, with ethylene as the main product.

The catalytic experiments performed in the presence of tetrahydrothiophene (THT) show however that NiMg is more deeply deactivated than Ni16, while BNi is only slightly more resistant to sulphur poisoning.

XRD, IR and TPR data suggest that the activating effect of Mg may be related to the competition of Mg^{2+} with respect to Ni^{2+} for the interaction with the alumina support surface. The previous deposition of Mg salt on the support, in fact, causes the penetration of Mg^{2+} into the alumina bulk forming a Mg$_x$Al$_2$O$_{3+x}$ subsurface layer, which limits the dispersion of Ni^{2+} favouring the formation of bigger NiO particles. After reduction, larger Ni particles are formed also favoured by the presence of CO that may favour building of larger particles through gas phase migration of Ni(CO)$_4$. The result is the formation of typically large Ni particles where CO adsorbs both on-top and in bridging configuration. This contrasts what happens with Ni/Al$_2$O$_3$ (Ni16) where very small Ni metal particles are found, where CO adsorbs in the on-top mode only.

Indeed, the possibility of building up large Ni particles has already been reported to allow lower temperature steam reforming activity. We showed previously that highly dispersed low loading Ni on alumina is also active in steam reforming of ethanol and phenol, but at higher temperature than high loading catalysts where larger Ni particles form [20]. Nevertheless, it seems also likely that the addition of Mg decreases the acidity of the uncovered alumina support, thus decreasing its activity in the main competitive reaction, i.e. ethanol dehydration.

The deposition of B after the support impregnation with Ni decreases the activity of the catalyst, but does not cause a definite decreasing of its steam reforming activity. Boron seems to reduce the amount of available Ni metal centers. In fact, according to IR experiments, while the isolated reduced Ni centers, which are producing polycarbonyls by CO adsorption, are fully killed by boron, also the amount of reduced Ni metal centers seems to be reduced with respect to Ni16. This likely occurs because of covering the Ni metal surface by borate species. This may be the main

effect in reducing the catalytic activity, with the total poisoning by borate species of part of Ni sites. The slight stabilizing effect towards sulphur poisoning might be due also to the reduced surface of Ni particles available to interact with sulphur, due to covering with borates, thus avoiding the formation of massive NiS.

In contrast, the deposition of boron before of Ni reduces significantly the catalytic activity. Part of this effect may be attributed to the larger exposition of the support (according to the larger size of NiO particles observed by XRD) and its slightly increased acidity, that favours ethanol dehydration with respect to steam reforming. However, it is evident that the conversion on NiB is definitely smaller than on Ni16, in spite of the similar size and characteristics of Ni metal particles apparent from IR and TPR experiments.

Actually, IR spectra suggest that the different activity of the catalysts may be associated also with the different adsorption and activation mode of water: data show that on NiMg catalyst water adsorbs largely in a non-dissociated structure more stable than on BNi catalyst, where adsorption is fully dissociative as typical of most ionic oxides. It seems possible, in agreement also with other authors [8], that water adsorption and activation may occur, at least in one of the most relevant steps, on the ionic uncovered support. Further studies are needed to check the role of water activation in steam reforming.

Acknowledgement

Appendix A. Supplementary data

Supplementary data associated with this article can be found, in the online version, at http://dx.doi.org/10.1016/j.apcatb.2013.09.030.

References

[1] J.R. Røstrup-Nielsen, K. Pedersen, J. Sehested, Appl. Catal. A: Gen. 330 (2007) 134–138.
[2] J. Kopyscinski, T.J. Schildhauer, S.M.A. Biollaz, Fuel 89 (2010) 1763–1783.
[3] http://www.axens.net/document/874/catalysts-a-adsorbents-catalogue/english.html
[4] S. Krupa, T. Foley, S. McColl, in: R.A. Meyers (Ed.), Handbook of Petrochemicals Production Processes, McGraw-Hill, 2005, p. 3, pp.11–14.
[5] http://www.uop.com/objects/KLP_60_Catalyst.pdf gr14
[6] J. Sehested, Catal. Today 111 (2006) 103–110.
[7] K. Aasberg-Petersen, I. Dybkjær, C.V. Ovesen, N.C. Schjødt, J. Sehested, S.G. Thomsen, J. Natural Gas Sci. Eng. 3 (2011) 423–459.
[8] N. Bion, D. Duprez, F. Epron, ChemSusChem 5 (2012) 76–84.
[9] W. Torres, S.S. Pansare, J.G. Goodwin Jr., Catal. Rev. Sci. Eng. 49 (2007) 407–456.
[10] M.M. Yung, W.S. Jablonski, K.A. Magrini-Bair, Energy Fuels 23 (2009) 1874–1887.
[11] D.A. Constantinou, M.C. Álvarez-Galván, J.L.G. Fierro, A.M. Efstathiou, Appl. Catal. B: Environ. 117–118 (2012) 81–95.
[12] P.F. Rossi, G. Busca, V. Lorenzelli, M. Waquif, O. Saur, J.C. Lavalley, Langmuir 7 (1991) 2677–2681.
[13] T. Montanari, L. Castoldi, L. Lietti, G. Busca, Appl. Catal. A: Gen. 400 (2011) 61–69.
[14] A.J. Vizcaíno, P. Arena, G. Baronetti, A. Carrero, J.A. Calles, M.A. Laborde, N. Amadeo, Int. J. Hydrogen Energy 33 (2008) 3489–3492.
[15] H.-S. Roh, K.Y. Koo, J.H. Jeong, Y.T. Seo, D.J. Seo, Y.-S. Seo, W.L. Yoon, S.B. Park, Catal. Lett. 117 (2007) 85–90.
[16] F. Basile, S. Albertazzi, D. Barbera, P. Benito, J. Einvall, J. Brandin, G. Fornasari, F. Trifiro', A. Vaccari, Biomass Bioenergy 35 (2011) S116–S122.
[17] J. Xu, L. Chen, K.F. Tana, A. Borgna, M. Saeys, J. Catal. 261 (2009) 158–165.
[18] W.J. Wang, M.-H. Qiao, H.X. Li, W.L. Dai, J.F. Deng, Appl. Catal. A 168 (1998) 151–157.
[19] G. Garbarino, E. Finocchio, G. Busca, V. Sanchez Escribano, Appl. Catal. B: Environ. 113–114 (2012) 281–289.
[20] G. Garbarino, A. Lagazzo, P. Riani, G. Busca, Appl. Catal. B: Environ. 129 (2013) 460–472.
[21] D.T. Beruto, R. Botter, A.W. Searcy, J. Am. Ceram. Soc. 70 (1987) 155–159.
[22] S. Brunauer, P.H. Emmett, E. Teller, J. Am Chem. Soc. 60 (1938) 309.
[23] C. Orr, J.M. Dalla Valle, Fine Particle Measurement, MacMillan, London, 1959, pp. 271.
[24] S. Brunauer, L.S. Deming, W.E. Deming, E. Teller, J. Am Chem. Soc. 62 (1940) 1723.
[25] J.H. De Boer, The Structure and Properties of Porous Materials, Butterworth, London, 1958, pp. 68.
[26] G. Paglia, C.E. Buckey, A.L. Rohl, R.D. Hart, k. Winter, A.J. Studer, B.A. Hunter, J.V. Hanna, Chem. Mater. 16 (2004) 220–236.
[27] G. Garbarino, S. Campodonico, A. Romero Perez, M.M. Carnasciali, P. Riani, E. Finocchio, G. Busca, Appl. Catal. A Gen. 452 (2013) 163–173.
[28] A. Delmastro, G. Gozzelino, D. Mazza, M. Vallino, G. Busca, V. Lorenzelli, J. Chem. Soc. Faraday Trans. 88 (1992) 2065–2070.
[29] M. García-Diéguez, E. Finocchio, M.Á. Larrubia, L.J. Alemany, G. Busca, J. Catal. 274 (2010) 11–20.
[30] K.I. Hadjiivanov, G.N. Vayssilov, Adv. Catal. 47 (2002) 307–511.
[31] M.B. Jensen, S. Moranti, F. Prinetto, A. Olafsen Sjastad, U. Olsbye, G. Ghiotti, Catal. Today 197 (2012) 38–49.
[32] F. Bentaleb, E. Marceau, Micropor. Mesopor. Mater. 156 (2012) 40–44.
[33] J.M. Rynkowski, T. Paryjczak, M. Lenik, Appl. Catal. A: Gen. 106 (1993) 73–82.
[34] B. Mile, D. Stirling, M.A. Zammitt, A. Lovell, M. Webb, J. Mol. Catal. 62 (1990) 179–198.
[35] M. Lindo, A.J. Vizcaino, J.A. Calles, A. Carrero, Int. J. Hydrogen Energy 35 (2010).
[36] J.C. Evans, Spectrochim. Acta 16 (1960) 1382–1392.
[37] G. Busca, G. Ramis, V. Lorenzelli, Stud. Surf. Sci. Catal. 55 (1990) 825–832.
[38] A. Popov, E. Kondratieva, J.P. Gilson, L. Mariey, A. Travert, F. Maugé, Catal. Today 172 (2011) 132–235.